POLITECNICO DI TORINO
Repository ISTITUZIONALE

Cascading Hazard Analysis of a Hospital Building

(Article begins on next page)

18 April 2024

1

CASCADING HAZARD ANALYSIS OF A HOSPITAL BUILDING

3

4 Sebastiano Marasco [1], Ali Zamani Noori [2], and Gian Paolo Cimellaro [3]

5 **ABSTRACT**

6 Recently, multi-hazards engineering has received more attention to analyzing the behavior of a

7 system exposed to different types of hazards and to estimate the loss data from cascading events

8 attributed to the primary hazard. In this paper, the principle of multi-hazards was investigated and a

9 new methodology was developed to assess the total damage of structural elements caused by

10 cascading hazards. For each hazard, a physical model is used to assess the conditional probability of

11 exceeding a certain intensity level due to the occurrence of the previous hazard. The method was

12 applied to a hospital located in California, US, subjected to the three cascading hazards (earthquake,

13 blast, and fire). Non-linear time-history analyses were performed using seven ground motions scaled

14 to five different earthquake levels and the seismic response of the structure was evaluated. The

15 seismic input produces damage to the hospital's power supply (Liquid Propane Gas reservoir tank)

16 which may cause a blast. The probability of explosion was estimated by taking into account the

17 probabilities of fuel leakage, fuel concentration, and ignition. A set of nine blast intensity levels was

18 considered in the analyses, corresponding to different quantities of fuel content inside the tank.

19 Afterward, a fire hazard is generated following the explosion, whose intensity level was evaluated

20 using the compartmental heat flux. The fire effects were modeled assuming an increment of

21 temperature in the steel frames. The proposed multi-hazard approach can be used for both improving

22 the structural safety and reducing the building life cycle costs to enhance in the end, the resilience of

[1] *Ph.D. Student, Department of Structural, Geotechnical and Building Engineering, Politecnico di Torino, Italy, E-mail: sebastiano.marasco@polito.it.*

[2] *Ph.D. Student, Department of Structural, Geotechnical and Building Engineering, Politecnico di Torino, Italy, E-mail: ali.zamani@polito.it.*

[3] *Visiting Professor, Department of Structural & Environmental Engineering, University of California, Berkeley, Berkeley, USA, E-mail: gianpaolo.cimellaro@polito.it.*

the hospital. Results show that this methodology can be used to provide risk mitigation measures within a more general resilience framework.

Keywords: Cascading hazards; Earthquake; Fire; Blast; Damage; Resilience.

INTRODUCTION

Latest disasters have shown that large parts of the world are subjected to multiple natural, manmade, and artificial hazards. The rising of global population and the massive economic development in areas prone to disasters have increased the chance of multiple catastrophic incidents, which lead to disruption of buildings and infrastructures. After realizing that multi-hazard cannot be averted, modern societies are trying to enhance their capacity to withstand and to minimize the impact of multi-hazard on community infrastructure and human beings. Therefore, multi-hazard engineering and related mitigation risks are prompting attention in the topic of design and retrofitting of buildings and infrastructures.

The concept of multi-hazard is defined as the "implementation of methodologies and approaches aimed at assessing and mapping the potential occurrence of different types of natural hazards in a given area. The employed methods have to take into account the characteristics of the single hazardous events as well as their mutual interactions and interrelations" (Delmonaco et al. 2006). Multi-hazard design starts with the structural and non-structural analysis for individual hazard. The location, magnitude, and frequency of occurrence of each hazard have to be estimated through a probabilistic approach. Several probabilistic approaches have been proposed for multi-hazard risk assessment. A quantitative risk analysis of industrial facilities in a seismic area was carried out by Fabbrocino et al. (2005) taking properly into account the multi-hazard effects. An oil storage plant with several atmospheric steel tanks containing flammable materials was considered as a case study. The vulnerability of the steel tanks was estimated through a quantitative probabilistic seismic risk analysis. The response of the industrial equipment was expressed in terms of limit states defined in accordance with the post-earthquake damage observations and the consequence analysis was

48 performed. Asprone et al. (2010) assessed the blast damage for a four-story reinforced concrete

49 building in addition to seismic fragility. A possible blast scenario was assumed during the service life

50 of a building located in a seismic zone, and then the probability of progressive collapse was

51 calculated using a Monte Carlo simulation procedure.

52 Recent evaluation of post-disaster effects has led to the implementation of significant changes in the

53 modeling and numerical assessment of multi-hazards. Padgett et al. (2010) evaluated hazard

54 intensities to accurately predict the vulnerability of bridges using a multivariate regression analysis

55 of the data obtained by surveys after Hurricane Katrina.

56 More specifically, when considering multi-hazard, the assessment has to be performed by comparing

57 risks of cascading mechanisms related to the triggered hazard event. For instance, the impact of an

58 earthquake on a gas pipeline may initiate gas leakage, which may likely cause an explosion. There

59 are several examples of sequential hazards initiated by earthquakes which have caused fire such as

60 San Francisco (1906), Tokyo (1923), Kobe (1995), and Northridge (1994) earthquakes (Usmani

61 2008). The risk assessment of structures that are exposed to more than one hazard is determined by

62 adopting the performance-based approach. Bruneau et al. (2006) investigated the performance of

63 steel piers under seismic action. The simulation of large-magnitude earthquakes and the consequent

64 explosions confirmed the capacity of the materials to resist to earthquakes and blast separately, but

65 not a simultaneous combination of the two hazards (Bruneau et al. 2006). A novel assessment

66 method was suggested by Barbato et al. (2013) to evaluate the individual impacts of the interaction

67 among hurricane wind, flood, windborne debris, and rainfall hazards in the Performance-Based

68 Hurricane Engineering (PBHE) framework.

69 Furthermore, disasters are catastrophic to the socio-economic activities and affected communities

70 (Lindell et al. 2006). Federal Emergency Management Agency (FEMA) developed HAZUS-MH

71 (2011) to perform multi-hazard analysis. It is capable of estimating economic, physical and social

72 effects by providing access to the average annualized loss and probabilistic results from the hurricane

73 wind, flood and earthquake models and combining them.

74   The combination of cascading hazards to evaluate the real performance of a structure is among the

75   most difficult tasks due to the intricacy involved in the process. Although the use of current

76   probabilistic approaches is perceived as an important instrument to quantify the total loss, developing

77   a simplified probabilistic methodology is clearly challenging. In this paper, a new approach to

78   estimate the total amount of structural damage caused by series of cascading hazards is proposed.

79   Earthquake, blast, and fire were considered as sequential hazards and numerical analyses were

80   performed to assess the fragility functions for each hazard. The combination of the structural damage

81   for cascading hazards was evaluated according to Bayes' theorem. The conditional probability of

82   exceeding a certain intensity level due to the occurrence of triggered hazard with a given intensity

83   level was estimated by using physical models that take into account the vulnerability of a structural

84   component. The methodology was applied to a steel structure hospital located in California, US.

85   The first section of the paper will provide a detailed description of the proposed methodology, while

86   the second part will illustrate its applicability through a case study building. Lastly, a numerical

87   example of total structural damage estimation is performed.

88   **PROPOSED METHODOLOGY**

89   The application of the multi-hazard approach can improve the safety of structures and minimize life

90   cycle costs and human losses. In the Performance-Based Earthquake Engineering (PBEE) framework

91   (Porter 2003), the structural performance is conventionally expressed in terms of probability to

92   exceed a stated performance objective when the structure is subjected to a certain level of hazard as

93   follow:

94    $$P(DV) = \iiint p(DV \mid DM) \cdot p(DM \mid EDP) \cdot p(EDP \mid IM) \cdot p(IM) \cdot dDM \cdot dEDP \cdot dIM \qquad (1)$$

95   where *DV* identifies the Decision Variable, *DM* represents the Damage Measure, *EDP* is the

96   Engineering Demand Parameter, and *IM* is the Intensity Measure that characterizes the hazard.

97   The term $p(IM)$ represents the density probability function of exceeding a certain IM for a given

98   hazard. In the case of cascading events, the correlation in terms of total exceedance probability of a

99   given IM ($P(IM_i \geq im_i)$) has to be estimated through the associated conditional probability (see Fig. 1).

100   $P(IM_i \geq im_i | IM_{i-1} \geq im_{i-1})$ represents the conditional probability of exceeding an IM for the ith hazard

101   ($IM_i \geq im_i$) due to a given IM for the $(i-1)^{th}$ hazard ($IM_{i-1} \geq im_{i-1}$).

102   In a multi-hazard scenario, the effects of different hazards combination (chain effects) have to be

103   considered. The damage caused by the occurrence of a hazard generates a degradation of the

104   Structural Parameters (SP) that influences the response of the structure subjected to the next

105   sequential hazard. The PBEE framework for multiple cascading hazards is shown in Fig. 2. To

106   consider the multi-hazard cascading effects, Eq. (1) can be rewritten as

107   $$P(DV) = \iiint p(DV|DM) \cdot p(DM|EDP) \cdot p(EDP|IM,SP) \cdot \left[\prod_{2}^{n} p(IM_i|IM_{i-1}) \right] \cdot p(IM_1) \cdot p(SP) \cdot dDM \cdot dEDP \cdot dIM_1 \cdot dSP$$

108   (2)

109   where IM_1 indicates the intensity measure parameter associated with the main hazard (triggered

110   hazard), the index i refers to i^{th} hazard, and n is the total numbers of cascading hazards.

111   Considering a multi-story building, the degradation of their structural characteristics (stiffness,

112   strength, and damping) is evaluated according to FEMA P440A (FEMA 2009) (see Fig. 3).

113   Assuming a rigid horizontal diaphragm, the general component of the reduced stiffness matrix is

114   calculated by

115   $$k_{f,jj} = 12 \cdot \frac{E_{f,j} \cdot I_j}{h_j^3} \tag{3}$$

116   where $k_{f,jj}$ is the reduced stiffness component, $E_{f,j}$ is the reduced elastic modulus, and I_j and h_j are the

117   inertia and height for the jth story, respectively. The damping matrix is evaluated according to the

118   Rayleigh formulation considering the reduced stiffness matrix.

119   The estimation of the probability of exceeding an IM for a hazard due to a given IM for the previous

120   hazard is provided by using specific physical models. As an example, a steel tank containing

121   flammable materials located in a seismic zone is considered. The probability to have an explosion of

122   the tank due to an earthquake with a given intensity level depends on the ignition mechanism of the

123   fuel content and on the failure modes of the tank. A physical model has to be capable of describing

124   the seismic fragility of the tank by identifying the most probable failure modes and the consequent

125   fuel release mechanism.

126   **CASE STUDY**

127   The case study considered earthquake, blast, and fire as series of cascading hazards. A five-story

128   steel building, located in Oakland, California, was designed according to the requirements of ASCE

129   7-10 (ASCE 2010). The basic building plan dimensions are 82.3 m (270 ft) by 33.7 m (110.5 ft),

130   with bays spanning of 9.1 m (30 ft) and 12.3 m (40.3 ft) in X and Y directions, respectively (see Fig.

131   4 and Fig. 5). The stories height is equal to 4.6 m (15 ft) and the structure was classified as regular in

132   both plan and elevation. The building is located on the relatively soft rock (site class C with

133   reference shear wave velocity ranging from 365.8 m/s (1200 ft/s) to 762 m/s (2500 ft/s) according to

134   ASCE 7-10 (ASCE 2010). The building has special steel moment resisting frame in the longest

135   direction (X-direction) and bracing system in the other direction (Y-direction). The designs of the

136   two considered lateral resisting systems are compliant with the code standards for design according

137   to the equivalent lateral force method (ASCE 2010). The W shape were used for beams and columns

138   while hollow structural sections (HSS) were designed for the bracing system (see Fig. 4 and Fig. 5).

139   The building's design comply with the occupancy category IV allowing the building to serve as a

140   hospital and accordingly an importance factor equals to 1.5 was considered in the seismic design.

141   The special steel moment resisting frame was designed with considering a response modification

142   factor (R) of 8 while the bracing system was designed with a response modification factor (R) of 6

143   considering the special steel concentrically braced frame according to ASCE 7-10 (ASCE 2010). The

144   P-Δ effects from the gravity columns were considered and the effects of large deformations of beam

145   and column elements were accounted for utilizing P-Δ nonlinear geometric transformation.

146   A standby power system was designed for providing an alternative source of electrical power for the

147   building and facilities in case of power outage. This system includes an above ground Liquid

148   Propane Gas (LPG) tank equipped with power sources, transfer equipment, controls, supervisory

149   equipment and accessory which are located outdoor. The tank was designed to provide a total power

150   of 2500 kVA and to maintain full capacity about 8 hours. The fuel capacity of the tank was assumed

151   equals to 718 l (190 gal) per hour at full load. Thus, the total LPG tank has a capacity of 3597 l (950

152   gal). The tank is 9.2 m (30 ft) away from the building according to National Fire Protection

153   Association (NFPA 2013). The Fig. 6 illustrates the geometric configuration of the LPG tank and

154   Fig. 7 shows its orientation with respect to the building.

155   The sequence of hazards triggered by the earthquake is not known and depends on the localization of

156   the high-risk potential elements inside and/or outside the analyzed structural system as well as their

157   level of damages. As an example, Fig. 8 represents the logical tree of multi-hazard sequence for

158   healthcare facilities.

159   The earthquake occurs and it causes damage to both building elements and external fuel tank. The

160   damaged tank may start fuel leakage and continues for a while in which gas ignites and causes

161   deflagration of the fuel inside the tank. Then, the explosion of the tank could generate an impulsive

162   air pressure load on the building façade which would cause localized damage to structural

163   components. The heat released by the tank explosion may cause the ignition of the inflammable

164   materials inside the buildings. In a short time, the ignition generates flashover and fire propagates

165   through the building compartment.

166   **HAZARD ANALYSIS**

167   **Earthquake**

168   The case study building is located in Oakland, California, US (Lat: 37.7792, Long: -122.1620).

169   Three hazard levels: 2%, 10%, and 50% probabilities of exceedance in 100 years were selected,

170   representing Collapse Prevention (CP), Life Safety (LS), and Immediate Occupancy (IO),

respectively (FEMA 2000). To better characterize the seismic hazard at the site, two additional sets of records representative of hazard levels at 5% and 20% probabilities of exceedance are also used in the analysis. The mean value of moment magnitude ($M_{W,mean}$) and epicenter distance (R_{mean}) with the logarithmic spectral offset at reference period ($\varepsilon(T_{ref})$) were evaluated according to Boore-Atkinson attenuation law (Boore and Atkinson 2008) for each Hazard Level (HL). All data can be found through the interactive de-aggregation of USGS (http://geohazards.usgs.gov/deaggint/2008/) (USGS 2013). The shear wave velocity at the uppermost 30 m has been assumed equal to 736 m/s (2415 ft/s) according to Global Vs30 Map Server (http://earthquake.usgs.gov/hazards/apps/vs30/) (USGS 2013). A new Ground Motion Selection and Modification (GMSM) procedure (Marasco and Cimellaro 2017) was used to minimize the dispersion values of the Engineering Demand Parameter (EDP) calculated through dynamic analyses. The new GMSM is based on the energy content in the frequency domain of the motions and it was carried out for the five HL. Seven groups of acceleration histories (for both horizontal directions) were selected for each HL in such a way to match the target spectrum at reference period of the building according to ATC P-58 (FEMA 2012). The Conditional Mean Spectrum (CMS-ε) obtained from the de-aggregation study was considered as target spectrum (Baker 2010). The Boore-Atkinson attenuation model (Boore and Atkinson 2008) was used to define the predicted spectral accelerations at the site (USGS 2013), while the Baker and Jayaram model was considered as correlation law (Baker and Jayaram 2010). Since the building is regular, the first period was selected as conditioning period (T_{ref}). The five CMS and the thirty-five groups of motions were obtained through the software OPENSIGNAL 4.1 (Cimellaro and Marasco 2015). A comparison between the target spectrum and the mean spectrum for HL of 2% and 5% in 100 years is depicted in Fig. 9 . For each HL, the mean spectrum was obtained as an average of the seven groups of spectra. The mean spectrum-compatibility is satisfied into the reference range of period (highlighted in grey in Fig. 9).

Furthermore, the spectral acceleration at reference period ($S_a(T_{ref})$) was considered as seismic IM parameter in the analyses. Table 1 resumes the values of the IM parameters for each HL obtained

197 from the CMS-ε spectra. The maximum value of spectral acceleration denotes a strong seismic action

198 that may occur with a 2% of probability of exceedance in 100 years.

199 **Blast**

200 After an earthquake, the supply system (fuel tank, electrical components, etc.) may be slightly or

201 severely damaged. Damage in the valves, connections or pipes of a fuel tank generates a fuel leakage

202 that may cause an explosion. If the fuel concentration is less than the flammable concentration range

203 or if the ignition sources are lacking, the explosion cannot occur. The three main factors influencing

204 the explosion occurrence are the fuel leakage, concentration of fuel, and ignition source. Thus,

205 considering the three parameters as stochastic variables, the total conditional probability of

206 exceeding an IM for blast ($IM_B \geq im_B$) due to a given IM for earthquake ($IM_E \geq im_E$) is expressed as

207 $$P(IM_B \geq im_B \mid IM_E \geq im_E) = P_L \cdot P_{FC} \cdot P_I \qquad (4)$$

208 where P_L represents the probability of fuel leakage, P_{FC} is the probability to have maximum fuel

209 concentration and P_I defines the probability of ignition.

210 Since the tank is relatively small in size, it is reasonable to assume that the damage occurs in the pipe

211 connected to the tank. According to ATC P-58-2 (FEMA 2012), the probability to have large gas

212 leakage for small diameter piping system (D<2.5 in) is given in terms of a fragility function with

213 accelerations as EDP (μ=1.1g, β=0.5). The probability to have maximum gas concentration was

214 estimated considering the pipe failure relative to the rigid joint connection. A simplified dynamic

215 model was developed to assess the maximum horizontal drift of the pipe.

216 The tank was considered as a rigid body upon shear flexible legs. The tank is fully restrained at the

217 base by the anchor bolts designed according to ASCE 7-10 (ASCE 2010).

218 The dynamic behavior of the tank depends on the Fuel Quantity (F_Q) inside the tank. This parameter

219 was considered as a stochastic variable normally distributed and nine different exceedance

220 probabilities were considered as shown in Table 2. Since the LPG tank has to supply energy in the

221 emergency conditions, its fuel quantity during an earthquake may not be less than a given minimum

222   threshold. In the case study, a normal distribution of the fuel quantity was assumed with a mean

223   value of 70% of the maximum quantity and standard deviation of 10. These parameters were selected

224   to accomplish a reasonable functionality of the supplying tank in case of emergencies. Since the tank

225   was designed to supply energy to the hospital in the case of power outage, the probability to have

226   low fuel volume was assumed close to zero. Furthermore, the exceedance probability to have 100%

227   of fuel quantity was fixed to 1.

228   Maximum fuel concentration (FC_{max}) is assumed to happen when the shear failure occurs in the

229   vertical pipe. According to this hypothesis and considering the maximum shear stress value on the

230   cross section of the pipe, the failure spectral acceleration ($S_{a,failure}$) is calculated by

231
$$S_{a,failure} = \frac{45.44}{g} \cdot \left(\frac{f_{u,d}}{E} \right) \cdot \left[\frac{L_v^3}{(D_e^2 - D_i^2)(D_e^2 + D_e \cdot D_i + D_i^2)} \right] \cdot \frac{1}{T_{tank}^2} \tag{5}$$

232   where $f_{u,d}$ and E represent the ultimate stress and elastic modulus of the steel, respectively, D_e and D_i

233   are the external and internal pipe diameter, and L_v is the length of the vertical pipe, and g is the

234   gravity acceleration.

235   The spectral acceleration at the reference period of the tank ($S_a(T_{tank})$) related to each selected ground

236   motion was considered as the first IM parameter (IM_1) and fuel quantity as the second IM parameter

237   (IM_2). Then, for each IM value, the spectral acceleration at the reference period of the tank was

238   compared with failure spectral acceleration. When $S_a(T_{tank})$ is greater than $S_{a,failure}$, the failure of the

239   pipe occurs and the probability to have maximum fuel concentration is assumed equal to 1 and 0

240   otherwise. Then, a tridimensional fragility surface was developed by fitting a lognormal distribution

241   of the obtained results.

242   Ignition probability is estimated according to the maximum released fuel quantity. The charts

243   provided by International Association of Oil and Gas Producers (IAOGP 2010) were used to estimate

244   the probabilities of hydrocarbon releases ignition for several scenarios. The total ignition probability

245   is considered as the sum of immediate and delayed ignition. Only delayed ignition probability was

246   considered in the case study since immediate ignition needs sources close to the fuel leakage point.

247   The release of flammable gases from small onshore LPG plant was considered as ignition scenario

248   according to IAOGP (IAOGP 2010) and the related probability function was assumed (see Fig.

249   10(c)).

250   The probability of gas leakage, maximum gas concentration, and ignition are shown in Fig. 10.

251   Maximum gas concentration (FC_{max}) was calculated according to the Bernoulli's principle assuming

252   failure of the pipe ($FC_{max}=29.70\ kg/s$) and the related probability was derived (see Fig. 10(c)).

253   Finally, the conditional probability of exceeding an IM for blast ($IM_B{\geq}im_B$) due to a given IM for

254   earthquake ($IM_1=Sa(T_{tank}){\geq}im_1,\ IM_2=F_Q{\geq}im_2$) is calculated by using Eq. (2) (see Fig. 11).

255   The fuel quantity does not have a considerable influence while the spectral acceleration at the period

256   of the tank provides a sensitive contribution especially for values greater than 0.5 g.

257   **Fire**

258   The probability to have fire inside the building is related to the heat transmission due to the tank

259   blast. Assuming the nine different exceedance probabilities for the fuel quantity, the heat flux (q_f) for

260   each point of the building in front of the tank was calculated according to the Stefan Boltzmann's

261   law. The combustion temperature of LPG was assumed equal to 2300 K° (Costin 2014), the

262   transmissivity coefficient in the atmosphere as 0.66, and the transfer configuration factor was

263   calculated for the entire external panel of the building (meshed with 0.5×0.5 m elements). Only the

264   opening surfaces (windows, doors, etc.) on the façade were considered as susceptible to trigger fire

265   inside the building. The internal walls are located between each two adjacent columns. Furthermore,

266   the ceiling and the internal walls of the building are composed by fireproof gypsum plasterboard

267   with steel studs. Thus, each fire compartment was identified as the volume confined between

268   adjacent columns (see Fig. 12) and ceiling.

269   The minimum value of heat flux capable of igniting the common flammable materials in a room was

270   assumed equal to 30 MJ/m^2 (Babrauskas and Krasny 1985). For each considered fuel quantity, the

271   surfaces of the building façade having a heat flux greater than 30 MJ/m^2 is identified (see Fig. 13).

272   The fire may propagate through the opening surfaces located within the heat flux surface for a given

273   fuel quantity (see Fig. 13) and the number and localization of the compartments under fire were

274   identified (see Table 3).

275   When the calculated heat flux is greater than the considered limit, the estimated conditional

276   probability to have ignition of elements inside the building was assumed equal to 1, and 0 otherwise.

277   The conditional probability of exceeding an IM for fire ($IM_F \geq im_F$) due to a given IM for blast

278   ($IM_B = F_Q \geq im_B$) was estimated ($P(IM_F \geq im_F | IM_B \geq im_B)$) by fitting a lognormal distribution of the

279   obtained results (see Fig. 14). A mean $\mu=40\%$ and standard deviation $\beta=0.95$ were estimated for the

280   lognormal cumulative density probability (see Fig. 14).

281
282   **SRTUCTURAL ANALYSIS**

283   **Earthquake**

284   The time history analyses were performed on a three-dimensional steel structure utilizing SAP2000

285   (Computers and Structures, Inc.). The nonlinearity of the structural elements was taken into account

286   according to concentrated plasticity model. According to FEMA 356 (FEMA 2000), *Steel-beams*

287   *Flexural Hinge* (type *Moment M3*) was used for beam elements while *Steel-column Flexural Hinge*

288   (type *P-M2-M3* with M-χ cylindrical domain) was applied for columns. The plastic hinges for brace

289   elements were modeled as *Steel-braces Axial Hinges*. 3% of damping ratio was assigned to the

290   frames using Rayleigh damping formulation with control frequency of 1.00 and 2.85 rad/s. The

291   nonlinear dynamic analyses were performed using non-linear direct integration method, taking into

292   account P-Δ effects and applying the horizontal acceleration time histories in the two principal plan

293   directions of the building model.

294   **Blast**

295   Estimation of blast load parameters was focused in the number of studies during the last decades and

296   several methods were proposed to determine the explosion wave properties. U.S. Army Technical

297   Manual (TM5-1300 1990) is a widely used standard which presents a series of charts to determine

298 the basic parameters of blast loads. Charts provided by TM5-1300 were used in order to establish the

299 blast load parameters required in structural analysis. As a general practice, the magnitude and

300 distribution of the blast load are a function of the quantity of output energy released by detonation,

301 charge weight (W), and the stand-off distance of explosive relative to the particular target (R). W is

302 expressed as an equivalent weight of trinitrotoluene (TNT) and blast wave demands were determined

303 in a function of universal scaled distance parameter ($Z = R/W^{1/3}$). TNT equivalent charge weight of

304 LPG fuel is given by (Sutton et al. 1975)

$$305 \qquad W_{TNT} = \varepsilon \frac{\Delta H_{C_{LPG}} W_{LPG}}{\Delta H_{c_{TNT}}} \qquad (6)$$

306 where W_{TNT} is TNT equivalent charge weight of LPG (kg), W_{LPG} is weight of LPG (kg), and $\Delta H_{C_{LPG}}$ is

307 LPG heat of combustion equals to 1.099×10^7 (cal/kg), $\Delta H_{C_{TNT}}$ is TNT heat of combustion equals to

308 1.109×10^6 (cal/kg). The unitless parameter ε is a term empirically equals to 0.1, and takes in account

309 the partial combustion and physical difference between TNT and gaseous explosion. In addition, an

310 empirical weight equivalency factor to consider the effect of the tank shell was considered as

311 (SBEDS 2008).

$$312 \qquad W_b = \left[0.2 + \frac{0.8}{\left(1 + W_c / W\right)} \right] W \qquad (7)$$

313 where W_b is equivalent bare charge weight (kg), W is charge weight inside casing (kg), and W_c

314 represents the weight of casing (kg). The spectral accelerations of the tank for each HL were

315 considered as first IM (IM_1), while nine different fuel quantities representative of the second IM

316 (IM_2) (ranging from 55% to 100%) were assumed for performing blast analyses were considered (see

317 Table 2).

318 Detonation of an explosive releases a large-scale of energy in terms of compressed air in a short

319 period of time (blast wave). Blast wave generates an instantaneous rise to the value of pressure (P_{so})

320 above ambient pressure (P_o). Then blast shock expands with very high velocity outward from the

13

321   explosion source into the surrounding areas (positive-pressure phase). As the blast wave travels into

322   increasingly larger areas, the energy of blast wave is dissipated and positive incident pressure at the

323   front decays. Within milliseconds of time, the air front pressure may drop below the normal

324   atmospheric pressure over the time period (t_o) which creates partial vacuums (negative-pressure

325   phase). The negative phase is usually of a longer duration (t_o-) than the positive phase and its

326   amplitude (P_{so}^-) is less than the ambient atmosphere pressure. When the blast wave encounters

327   structure, reflection increases the overpressure to a maximum pressure (P_r) which is greater than the

328   peak incident pressure (P_{so}) (see Fig. 15(a)).

329   The reflected pressure is a function of the incident angle (between the shock wave and the line

330   perpendicular to the target surface) and the incident pressure. The maximum reflected pressure and

331   corresponding total reflected impulse (i_r) were calculated through provided charts by TM5-1300. For

332   design purpose, the blast time history overpressure was idealized by rising of an equivalent triangular

333   pulse of maximum reflected pressure at an arrival time (t_A) after the explosion (see Fig. 15(b)). The

334   actual positive duration was replaced by a fictitious duration (t_{rf}) assuming the linear decay of

335   overpressure is given by (TM5-1300 1990)

336
$$t_{rf} = 2i_r / P_r \tag{8}$$

337   A similar procedure for determining the negative fictitious duration (t_{rf}^-) was used whereas rising

338   time of negative peak pressure is considered equal to $0.25 \cdot t_{rf}^-$. Different blast pressure time histories

339   specific to each member were established corresponding to the different scaled distance parameter

340   (Z) and potential charge weight for each blast IM.

341   The blast load was applied to beams, columns and exterior walls on the exposed structural area on

342   the front face of the explosion. The reflection areas of the building were assumed big enough in order

343   that there is no blast wave diffraction around the structure. Exterior walls were considered as typical

344   concrete masonry wall reinforced with vertical bars. Since the vertical span of the wall is less than

345   the horizontal span, and also the connection between the wall and adjacent columns are typically

346   weak, the most of the wall strength and stiffness is provided by the vertical direction. Hence the wall

14

347   components were considered as one-way spanning elements that can transfer only the equivalent

348   static reaction load to the adjacent beams.

349   To do blast analysis, each wall was simplified as a Single Degree Of Freedom (SDOF) system. The

350   mass, stiffness and actual force of the wall were transformed into an equivalent system so that the

351   deflection of the concentrated mass is the same as the mid-span of the actual wall (Biggs 1964). An

352   elasto-perfectly plastic behavior for the wall was considered taking into account its dynamic

353   characteristics under the high-velocity impacts (TM5-1300). The dynamic responses of the mid-span

354   of the wall, considering the plastic hinge development (yield rotation capacity), were determined.

355   Resulted time history reactions were calculated and directly applied to the adjacent beams in

356   SAP2000 models (Computers and Structures Inc.) considering the rigid diaphragm for each floor.

357   For the columns and beams, blast pressure time histories were determined and the corresponding

358   pressures-time functions were applied directly on framing elements. The structural stiffness

359   reduction caused by the earthquake was assessed according to FEMA P440A (FEMA 2009)

360   degradation model. For each seismic IM, the mean values of stiffness reduction for the selected

361   seven groups of ground motions were considered.

362   Mechanical properties of steel materials were enhanced by means of Dynamic Increased Factors

363   (DIF) in order to take into account the effects of high rapid load environment compared to static

364   loading conditions (TM5-1300 1990). Since the blast load duration is very short compared to the

365   fundamental natural period of the structure, the structural damping effects were not considered in the

366   analyses. Transmission of the ground shock induced by the explosion to the foundation of the

367   structure was not considered in this study. Finally, nonlinear time history analyses were carried. In

368   the cases of the loss of the load-bearing capacity of key structural components, the progressive

369   collapse analyses were performed and the dynamic effects of removal of the failed elements were

370   evaluated using time history analyses.

371   **Fire**

372   After ignition of inflammable materials inside the compartment, flashover occurs causing an increase

373   in temperature. Design-basis fire standards are based on the evaluation of post-flashover time-

374   temperature relationships (fire curve) for the compartment. Naturally, the fire curve depends on the

375   quantity of combustible materials (total calorific value), the velocity of combustion, and the

376   ventilation conditions. The first two parameters affect the total heat flux generated within the

377   compartment (q_f). According to Euro Code 1 (EC1, 2002), the specific fire load is given in terms of

378   mean value and standard deviation of a normally distributed function for different building

379   categories. For hospitals, the mean specific fire load of 230 MJ/m^2 and the standard deviation of 69

380   are suggested. In the study case, the specific heat flux of the compartment was selected as first IM

381   (IM$_1$) and eight different exceedance probabilities were considered as shown in Table 4.

382   The fuel quantity inside the tank was assumed as second IM parameter (IM$_2$).

383   Since temperature-time relationships are not suitable to describe the real post-flashover behavior

384   (growth phase, steady-burning phase, and decay phase), several idealized temperature-time functions

385   were developed. In this study, the temperature-time relationship developed by Lie (Lie et al. 1974)

386   was considered as given below

387
$$
\begin{cases}
T = 250 \cdot (10 \cdot F)^{0.1/F^{0.3}} \cdot \exp(-F^2 \cdot t) \cdot [3 \cdot (1 - \exp(-0.6 \cdot t)) + \\
- (1 - \exp(-3 \cdot t)) + 4 \cdot (1 - \exp(-12 \cdot t))] + C \cdot \left(\dfrac{600}{F} \right)^{0.5} \\
T = -600 \cdot \left(\dfrac{t}{t_{peak}} \right) - 1 + T_{peak}
\end{cases}
\tag{9}
$$

388   The first expression describes the heating phase, while the second one is referred to the cooling

389   phase. The ventilation conditions are considered by means of the opening factor F

390   ($F = A_v \cdot (H)^{0.5} / A_c$), where A_v is the total surface of vertical openings, H is the height of openings,

391   and A_c is the area of the compartment. Two vertical openings with 1.50 m×2.00 m were assumed for

392   each compartment (see Fig. 12) and the opening factor of 0.07 was calculated.

393   The constant C is associated with the type of burned materials and it is assumed equal to 1 for light

394   materials and 0 for heavy ones. The top of the curve is described by peak time (t_{peak}) and peak

395   temperature (T_{peak}). These two parameters define the fire severity inside the compartment. These

396   parameters were defined according to the time equivalence concept, that relates the real fire exposure

397   to the standard test fire (standard curve). EC1 (EC1 2002) proposes the calculation of the equivalent

398   time t_e expressed as

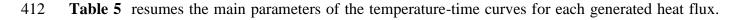399 $$t_e = k_b \cdot w \cdot q_f \tag{10}$$

400   where q_f is the fire load in terms of heat flux and k_b is a parameter taking into account the different

401   compartment lining (generally equal to 0.07 min m^2/MJ). Considering only vertical openings in

402   compartment, the ventilation factor w is given by

403    $$w = \left(\frac{6}{H_c}\right)^{0.3} \cdot \left[0.62 + 90 \cdot \left(0.4 - \frac{A_v}{A_c}\right)^4\right] \tag{11}$$

404   where H_c defines the height of the compartment.

405

406

407

408

409

410

411

412   **Table 5** resumes the main parameters of the temperature-time curves for each generated heat flux.

413   According to the obtained results listed in

414

415

416

417

418

419

420 **Table 5**, the slope of the heating curve (T_{peak}/t_{peak}) decreases with the increasing of the generated heat

421 flux into the compartment.

422 Degradation of the physical and mechanical characteristics of the materials and the actions due to the

423 fire were evaluated. According to Fourier's equation, the thermal distribution depends on the net

424 transmitted heat flux ($q_{f,n}$) in the time for a given fire scenario. Assuming all the structural elements

425 as homogeneous and isotropic, the Fourier's problem can be integrated into the volume of the

426 element and rewritten in the discrete form as (EC3 2005)

$$\Delta T_{(i)} = k_{sh} \cdot \frac{A_m / V}{\rho \cdot c} \cdot q_{f,n(i)} \cdot \Delta t \qquad (12)$$

428 where $\Delta T_{(i)}$ defines the ith increment of uniform temperature in the element cross section and A_m/V is

429 the section factor given by the ratio between the area of the element exposed to fire (A_m) and its total

430 volume (V). Density (ρ) and specific heat (c) are referred to the material composing structural

431 element while Δt is the time step in which the increase of temperature occurs ($\Delta t < 5s$). The fire

432 protection system effect was neglected in the fire analysis. The current fire codes do not address the

433 compound effects of hazards in a sequential manner. In fact, the damage to structural elements due to

434 earthquake and blast, causes partial loss of fire protection (e.g. cracking of fireproof cladding,

435 peeling of fireproof painting, etc.). Since in this case study, the fire load was applied on the structure

436 damaged by sequential earthquake and blast, all the measures for fireproofing are deteriorated. The

437 estimation of fire protection loss percentage is out of this study, then the total loss of fireproof

438 system was considered as the worst case.

439 The coefficient k_{sh} takes into account the "shadow effects" that is responsible for a non-uniform

440 thermal transversal distribution. In order to consider a pseudo-uniform transversal temperature

441 distribution, the k_{sh} coefficient was considered according to the real fire exposure. Parameter $k_{sh}=0.7$

442 was assumed for beams (fire exposure on three sides) and $k_{sh} = 0.9 \cdot \left(A_m / V\right)_b / \left(A_m / V\right)$ was

443   considered for columns according to Eurocode 3 (EC3 2005). The ratio $(A_m/V)_b$ is the section factor

444   of the element that was assumed as bin section and (A_m/V) is the real section factor of the column.

445   The fire exposure for the column was supposed for one side of the web and for both flanges. Three

446   different section of beams and columns have been identified for the compartment. Table 6

447   summarizes the uniform temperature on the steel cross sections of the compartment at t_{peak} time for

448   each heat flux value where the sections W12x136 and W14x109 identify the columns and the section

449   W21x44 is related to the beams inside the compartments.

450   Fire resistance of steel elements inside the compartment was evaluated considering the maximum

451   uniform thermal loads for each heat flux value. The software SAP2000 (Computers and Structures

452   Inc.) was used to perform the analyses. The mechanical and physical materials properties were

453   modified according to AISC (AISC 2005) depending on the temperature value. The nonlinearity of

454   the structural elements was taken into account according to concentrated plasticity model and the

455   progressive nonlinear analyses were performed. The structural stiffness reduction caused by the

456   earthquake and blast was assessed according to FEMA P440A (FEMA 2009) degradation model. For

457   each seismic IM the mean values of stiffness reduction for the selected seven groups of ground

458   motions were considered. The reduced stiffness, strength, and damping were also calculated for each

459   selected fuel quantity value.

DAMAGE ANALYSIS

Earthquake

462   A common approach is to correlate the performance of structural elements to one or more EDPs

463   based on peak inter-story drifts. Peak inter-story drifts are capable of providing information about

464   the damage state of the elements. According to ATC P-58 (FEMA 2012), four Earthquake Damage

465   States (DS_E) (slight, moderate, extensive, and complete) have been identified for the steel building

466   depending on the transient drift ratio. The associated fragility curves are provided for both horizontal

467   directions using the four DS_E (see Fig. 16).

468 **Blast**

469 In blast analyses, the evaluation of the structural building performance based on inter-story drifts

470 limits the investigation to maximum local damage. The blast causes a damaged localized on the

471 structural components depending on the distance to the blast source. In the case of intense blast load,

472 a partial collapse may occur causing a redistribution of the actions in the slightly damaged

473 components. Thus, the estimation of the damage on a building has to take into account the global

474 behavior of the structure. In order to accurately assess the global response of a building under blast

475 load, the loss of horizontal stiffness was assumed as EDP. The evaluation of the structural global

476 response requires the maximum lateral displacements shape of the building due to the blast and the

477 total induced elastic action. In the case study, the response of the structure in Y direction (see Fig. 5)

478 was assimilated to a SDOF dynamic response given by

479
$$K_{eq} = \frac{\delta_{eq}}{V_{eq}} = \frac{\delta_{top} \cdot \sum_{i=1}^{N=5} \left(\phi_i - \phi_{i-1} \right)^2}{V_b \cdot \sum_{i=1}^{N=5} \phi_i} \tag{13}$$

480 where δ_{top} is the maximum top floor displacement and V_b is the base shear resulted at the same time

481 of the maximum displacement. The real distribution of floor displacements was taken into account

482 through the shape coefficients ϕ_i that represents the ith floor displacement normalized with respect

483 the top one. Table 7 resumes the horizontal stiffness reduction for each selected fuel quantity level

484 derived from the performed progressive collapse analyses. The lateral stiffness reduction was

485 calculated for each selected earthquake scenario considering the chain effects. Thus, the degradation

486 of the structural parameters was evaluated and the blast load was applied on the structure with

487 modified mechanical characteristics. The first column of Table 7 represents the five different HLs for

488 earthquake while the first row identifies the nine HLs selected for the fuel quantity.

489 The yield drift for the braced system was calculated according to ATC P-58 (FEMA 2012) and the

490 maximum drift threshold was assumed for four different damage states. The stiffness reduction limits

491 were calculated assuming an elasto-perfectly plastic global behavior of the steel frame (see Table 7).

20

492 According to the estimated stiffness reduction values for each damage state, the associated

493 exceedance probability ($P(DS_B \geq ds_B)$) surfaces were evaluated (see Fig. 17).

494 **Fire**

495 The structural capacity assessment was carried out considering maximum deflection for beams and

496 columns as EDP. Two different damage states were assumed:

497   -   Fire Damage State 1 ($DS_{F,1}$): irreversible damage on the beam with maximum response;

498   -   Fire Damage State 2 ($DS_{F,2}$): irreversible damage in the column with maximum response.

499 The first damage state gives information about the maximum flexural capacity of the beam. The

500 threshold vertical deflection (v_b) for this damage state was assumed equal to the deflection causing

501 an uncontrolled vertical displacement (Gernay et al. 2016). The second damage state is related to the

502 maximum drift of the column (δ_c) under multiple stresses due to compression and bending moment,

503 taking into account the P-Δ effects. The maximum limit for the drift was assumed coincident with the

504 horizontal displacement that produces uncontrolled unstable displacement (Gernay et al. 2016).

505 Several analyses were performed considering the different fuel quantity and heat ratio as HLs. The

506 degradation of the structural parameters was evaluated and the fire load was applied on the structure.

507 For each analysis, the probability to have irreversible damage to the structural elements was assumed

508 equal to 1 if the response parameter is greater than the associated limit and 0 otherwise.

509 The probability of exceeding certain damage state due to the fire hazard ($P(DS_F \geq ds_F)$) was developed

510 fitting lognormal distribution to the obtained data (see Fig. 18).

511 <div align="center">**NUMERICAL EXAMPLE**</div>

512 The total probability of exceeding a given damage state was derived according to Eq.(2). In a

513 cascading multi-hazard scenario, the probability of exceeding a given damage state has to be

514 calculated considering the conditional probability of exceeding a certain intensity level due to the

515 occurrence of the previous hazard. For the case study, earthquake-blast-fire was considered as

516 cascading hazards. According to the numerical analyses performed and considering a complete

517 damage to the columns of the building as damage state, the probabilities of exceeding the selected

518 level of damage was estimated for the three hazards.

519 The spectral acceleration at the period of the structure, fuel quantity inside the tank, spectral

520 acceleration at the period of the tank, and heat flux generated in the compartment were assumed as

521 IM parameters. A numerical example was carried out with reference to the five different HL for the

522 earthquake, 80% of the full capacity of the tank and heat flux equal to the average value. Table 9

523 shows exceedance damage probability values for the case study building and the conditional

524 probability of exceeding an IM for the one hazard due to a given IM for the previous hazard. The

525 complete damage on the columns was selected as damage state and then the associated exceedance

526 damage probability ($P(DS>ds)$) was estimated.

527 It is clear that the probability to have blast after the earthquake is correlated to the size of the tank. In

528 the case study, a low conditional probability of exceeding an IM for the blast due to a given IM for

529 the earthquake was associated with the value of maximum gas concentration. But, for the cases of

530 farm tanks, the conditional probability value may be considerable.

531   **CONCLUDING REMARKS**

532 Recent experiences have shown that buildings and infrastructures are significantly vulnerable to

533 multi-hazard effects. The combination of cascading hazards is essential to evaluate the real

534 performance of a structure and the respective economic losses. This study presented a new approach

535 to assessing the conditional probability of exceeding a certain intensity level due to the occurrence of

536 the previous hazard, estimating the exceedance damage probability and taking into account the

537 interdependency between different hazards. The main novelty of this research is the estimation of

538 exceedance damage probability for a given damage state due to earthquake, blast and fire hazard by

539 considering the physical models. The method can be considered as an alternative to the Monte Carlo

540 simulations, thus it reduces the computational time to perform the analyses, but it requires accurate

541 calibration of the physical parameters which plays a key role in reducing the epistemic uncertainty of

542   the model. In addition, the degradation of the structural parameters was taken into account for

543   correctly assessing the performance of a structure subjected to cascading hazards.

544   The application of the proposed cascading multi-hazard approach can be used for both improving the

545   structural safety and reducing the building life cycle costs to enhance the resilience of the structure.

546

551

552

553

554   **References**

555   AISC (2005). "Specification for Structural Steel Buildings." AISC 360, American Institute of Steel

556   Construction, Chicago, IL.

557   ASCE. (2010). "Minimum design loads for buildings and other structures." 7-10, Reston, VA.

558   Asprone D., Jalayer F., Prota A., and Manfredi G. (2010). "Proposal of a probabilistic model for

559   multi-hazard risk assessment of structures in seismic zones subjected to blast for the limit

560   state of collapse." *Structural Safety*, Volume 32, Issue 1, Pages 25-34.

561   ATC (2012). "Seismic Performance Assessment of Buildings." *ATC-58, Applied Technology*

562   *Council,* Redwood City, CA.

563   Babrauskas V., and Krasny J.F. (1985). "Fire Behaviour of Upholstered Furniture." *NBS*

564   *Monograph* 173 (U.S.), National Bureau of Standards.

565   Baker, J. W. (2010). "Conditional mean spectrum: Tool for ground-motion selection." *Journal of*

566   *Structural Engineering*, 137(3), 322-331.

567   Baker, J. W., and Jayaram, N. (2008). "Correlation of spectral acceleration values from NGA ground

568   motion models." *Earthquake Spectra*, 24(1), 299-317.

569   Barbato, M., Petrini, F., Unnikrishnan, V. U., and Ciampoli, M. (2013). "Performance-Based

570   Hurricane Engineering (PBHE) framework." *Structural Safety*, 45, 24-35.

571   Biggs, J. M. (1964). *Introduction to structural dynamics*, McGraw-Hill, New York.

572   Boore, D. M., and Atkinson, G. M. (2008). "Ground-motion prediction equations for the average

573   horizontal component of PGA, PGV, and 5%-damped PSA at spectral periods between 0.01 s

574   and 10.0 s." *Earthquake Spectra*, 24(1), 99-138.

575   Bruneau, M., Lopez-Garcia, D., and Fujikura, S. "Multihazard-resistant highway bridge bent." *Proc.,*

576   *Proc., Structures Congress*, ASCE New York, 1-4.

577   Cimellaro, G. P., and Marasco, S. (2015). "A computer-based environment for processing and

578   selection of seismic ground motion records: Opensignal." *Frontiers in Built Environment*, 1,

579   17.

580   Computer and Infrastructure Inc. SAP2000, Version 17.3, Berkeley, CA.

581   Costin, N. S. (2014). "Numerical simulation of detonation of an explosive atmosphere of liquefied

582   petroleum gas in a confined space." Defence Technology, 10(3), 294-297.

583   Delmonaco, G., Margottini C., and Spizzichino D. (2006). "Report on new methodology for multi-

584   risk assessment and the harmonisation of different natural risk maps." *Deliverable 3.1,*

585   *ARMONIA*.

586   EC (2002). "Eurocode 1: Actions on structures." *Part 1-1: General actions - Densities, self-weight,*

587   *imposed loads for buildings*, EC1, European Committee for Standardization, Bruxelles, BG.

588   EC (2005). "Design of steel structures - Part 1-2: General rules -Structural fire design." *EC3,*

589   *European Committee for Standardization,* Bruxelles, BG.

590   Fabbrocino G., Iervolino I., Orlando F., and Salzano E. (2005)."Quantitative risk analysis of oil

591   storage facilities in seismic areas." *Journal of Hazardous Materials*, Volume 123, Issues 1–3,

592   Pages 61-69.

593   FEMA (2000). "Prestandard and Commentary for the Seismic Rehabilitation of Buildings." FEMA

594   356, Federal Emergency Management Agency, Washington, D.C.

595   FEMA (2009). "Effects of Strength and Stiffness Degradation on Seismic Response." FEMA P440A,

596   Federal Emergency Management Agency, Washington, D.C.

597   FEMA (2011). "Hazus FEMA's methodology for estimating potential losses from disasters ", FEMA

598   Federal Emergency Management Agency, Washington, D.C.

599   Gernay, T., Khorasani, N. E., and Garlock, M. (2016). "Fire fragility curves for steel buildings in a

600   community context: a methodology." Engineering Structures, 113, 259-276.

601   IAOGP (2010). "Ignition probabilities." *Risk Assessment Data Directory*, International Association

602   of Oil & Gas Producers, Report No. 434-6.1.

603   Lie, T. T. (1974). "Characteristic temperature curves for various fire severities." *Fire Technology,*

604   *4pp. 315-326*.

605   Lindell, M. K., Perry, R. W., Prater, C., and Nicholson, W. C. (2006). "Fundamentals of emergency

606   management". Washington, DC: FEMA. Chicago.

607   Marasco, S., Cimellaro, G.P. (2017). "A new energetic based ground motion selection and

608   modification algorithm.". Proc., 16th World Conference on Earthquake Engineering,

609   Santiago, Chile.

610   NFPA 30 (2013). "Flammable and Combustible Liquids Code." Committee on Tank Storage and

611   Piping Systems.

612   Padgett, J., Ghosh, J., and Ataei, N. (2010). "Sensitivity of dynamic response of bridges under

613   multiple hazards to aging parameters." *Proc., 19th analysis and computation specialty*

614   *conference. ASCE*.

615   Porter, K.A. (2003). "An overview of PEER's performance-based earthquake engineering

616   methodology." *Proc. Ninth International Conference on Applications of Statistics and*

617   *Probability in Civil Engineering (ICASP9)* July 6-9, 2003, San Francisco, CA. Civil

618   Engineering   Risk   and   Reliability   Association   (CERRA),   973-980.
619   http://www.sparisk.com/pubs/Porter-2003-PBEE-Overview.pdf.

620   SBEDS (2008). "Methodology Manual for the Single-Degree-of Freedom Blast Effects Design
621   Spreadsheets." *PDC TR-06-01 Rev 1*, Protective Design Center Technical Report, U.S. Army
622   Corps of Engineers.

623   Sutton, S. B., and McCauley, E. W. (1975). "Assessment of Hazards Resulting from Atmospheric
624   Propane Explosions at Lll.", US Energy Research and Development Administration,
625   California Univ., Livermore Lawrence Livermore Lab.

626   TM5-1300 (1990). "The Design of Structures to Resist the Effects of Accidental Explosions."US
627   Department of the Army, Navy, and Air Force, Washington DC.

628   USGS   (2013).   "Seismic   Hazard   Analysis   tools.   U.S.   Geological   Survey."   <
629   http://earthquake.usgs.gov/hazards/designmaps/grdmotion.php>.

630   Usmani, A. S. (2008). "Research priorities for maintaining structural fire resistance after seismic
631   damage". In Proceedings of the 14th world conference on earthquake engineering, Beijing.

632

633

634

635   **Fig. 1.** Conditional probabilities for cascading hazards

636   **Fig. 2.** Performance-Based earthquake Engineering for cascading hazards scenario

637   **Fig. 3.** Cyclic degradation for structural elements (FEMA P440A 2009)

638   **Fig. 4.** Lateral moment resisting frame configuration

639   **Fig. 5.** Internal bracing frame configuration

640   **Fig. 6.** Geometric configuration of the LPG tank

641   **Fig. 7.** LPG tank orientation with respect to the building façade

642   **Fig. 8.** Example of hazard sequence: earthquake-blast-fire

643   **Fig. 9.** (a) mean spectrum compatibility for 2% of exceedance probability in 100 years, (b) 5% of
644   exceedance probability in 100 years (reference range of period highlighted in grey)

645   **Fig. 10.** (a) probability to have leakage, (b) probability to have maximum fuel concentration, (c)
646   probability of ignition (according to IAOGP, 2010)

647   **Fig. 11.** Conditional probability of exceeding an IM for blast ($IM_B \geq im_B$) due to a given IM for
648   earthquake ($IM_1 = Sa(T_{tank}) \geq im_1$, $IM_2 = F_Q \geq im_2$)

649   **Fig. 12.** Fire compartments division for the building plan

650   **Fig. 13.** Building façade having a heat flux greater than 30 MJ/m^2 for each fuel quantity value

651   **Fig. 14.** Conditional probability of exceeding an IM for fire ($IM_F \geq im_F$) due to a given IM for blast
652   ($IM_B = F_Q \geq im_B$)

653   **Fig. 15.** (a) blast overpressure-time history for a face-on reflected wave; (b) idealized blast
654   overpressure time history (adopted by TM5-1300 1990)

655   **Fig. 16.** (a) Probability of exceeding a given damage state for earthquake hazard ($P(DS_E \geq ds_E)$) in X
656   direction; (b) Y direction

657   **Fig. 17.** (a) Probability of exceeding a slight, (b) moderate, (c) extensive, (d) complete damage state
658   for blast hazard ($P(DS_B \geq ds_B)$)

659   **Fig. 18.** (a) Probability of exceeding a irreversible damage on the beams, (b) irreversible damage on
660   the columns for fire hazard ($P(DS_F \geq ds_F)$)

661

662

663

664

665

Table 1. IM parameters values for earthquake

$P_{VR,E}$ [%]	50	20	10	5	2
$Sa(T_{ref})$ [g]	0.20	0.41	0.58	0.76	1.00

Note: $P_{VR,E}$ is the exceedance probability in 100 years for earthquake hazard.

666

Table 2. Selected exceedance probability for fuel quantity and associated values.

P_{FQ} [%]	90	75	65	50	20	10	5	2	1
Fuel quantity [%]	55	62	67	70	77	80	86	92	100

Note: P_{FQ} is the fuel quantity exceedance probability.

Table 3. Number and localization of the compartments under fire for each fuel quantity value.

P_{FQ} [%]	90	75	65	50	20	10	5	2	1
Fuel quantity [%]	55	62	67	70	77	80	86	92	100
Compartment area ID	C5 C14	C5 C14	C5 C14	C4 C5 C6 C13 C14 C15	C4 C5 C6 C13 C14 C15	C4 C5 C6 C13 C14 C15	C4 C5 C6 C13 C14 C15	C4 C5 C6 C13 C14 C15	C4 C5 C6 C13 C14 C15
Compartment height ID	H1	H1	H1	H1	H1 H2	H1 H2	H1 H2	H1 H2	H1 H2

Note: P_{FQ} is the fuel quantity exceedance probability.

667

Table 4. Selected exceedance probability for each generated heat flux.

P_{qf} [%]	90	85	80	50	20	10	5	2
q_f [MJ/m^2]	135	160	180	230	281	322	360	400

Note: P_{qf} is the compartmental heat flux exceedance probability.

668
669

670

671

672

673

674

28

Table 5. Characteristic time-temperature curve parameters for each generated heat flux.

P_{qf} [%]	90	85	80	50	20	10	5	2
t_e [min]	23.50	25.00	26.19	33.46	40.83	46.85	52.2	58.2
T_{peak} [K°]	1111	1131	1145	1173	1188	1205	1218	1228
t_{peak} [min]	11.5	13.5	16	20.5	24.5	29.5	33.5	37

Note: P_{qf} is the compartmental heat flux exceedance probability.

Table 6. Uniform temperature in the cross section of the structural elements within the compartments.

		P_{qf} [%]							
	Element	90	85	80	50	20	10	5	2
ΔT_{MAX} [K°]	W21x44	677	777	846	925	971	1,019	1057	1089
	W14x109	635	729	794	867	911	956	991	1021
	W12x136	560	643	700	765	804	843	875	901

Note: P_{qf} is the compartmental heat flux exceedance probability.

Table 7. Percentage of the stiffness reductions for each fuel quantity and earthquake HLs.

		P_{FQ} [%]								
		90	75	65	50	20	10	5	2	1
$P_{VR,E}$ [%]	50	62.28	71.96	74.63	76.89	87.5	92.77	96.53	97.20	98.98
	20	65.32	74.12	77.03	78.29	89.13	94.73	97.66	98.22	100.00
	10	68.76	79.74	80.83	85.18	93.19	98.52	99.83	99.75	100.00
	5	72.33	84.16	87.44	91.28	98.36	99.79	100.00	100.00	100.00
	2	79.52	89.59	93.89	97.85	100.00	100.00	100.00	100.00	100.00

Note: $P_{VR,E}$ is the exceedance probability in 100 years for earthquake hazard and P_{qf} is the compartmental heat flux exceedance probability.

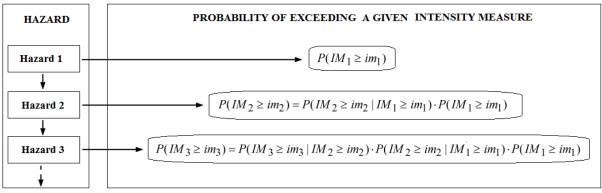**Table 8.** Blast Damage States and calculated stiffness reduction for blast analysis.

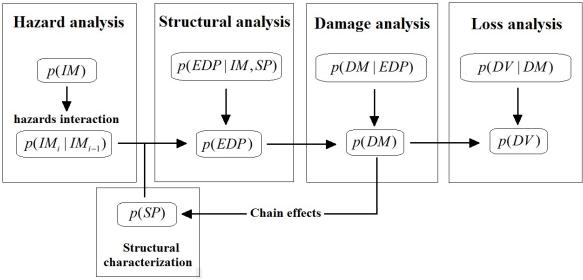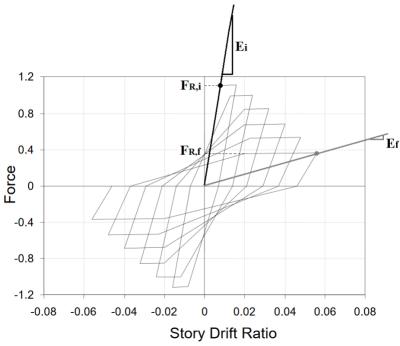| Blast Damage State (DS_B)	Slight	Moderate	Extensive	Complete
Drift [%]	1.00	1.80	2.80	4.80
Stiffness reduction [%]	30.00	61.00	75.00	85.00

682 **Table 9.** Numerical example for exceedance damage probability calculation due to earthquake, blast
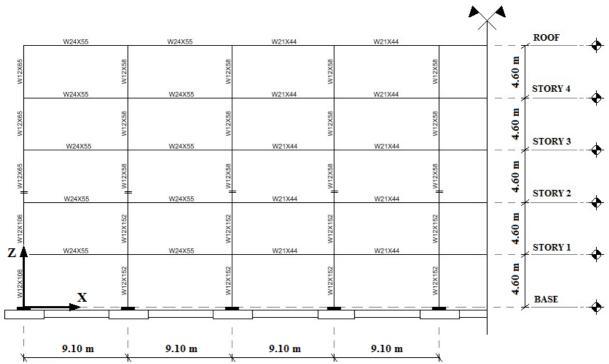683 and fire hazards, considering complete damage on the columns.

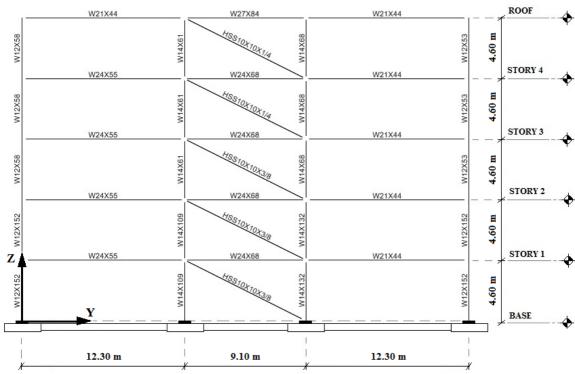| $P_{VR,E}$ [%]	$Sa(T)$ [g]	$Sa(T_{tank})$ [g]	$P(IM_B>im_B|IM_E>im_E)$ [%]	$P(IM_F>im_F|IM_B>im_B)$ [%]	$P(DS_E>ds_E)$ [%]	$P(DS_B>ds_B)$ [%]	$P(DS_F>ds_F)$ [%]	$P(DS>ds)$ [%]
2	1,00	0.95	3.80	80.00	100.00	100.00	82.00	100.00
5	0.75	0.85	1.60	80.00	80.00	98.00	82.00	82.62
10	0.55	0.75	1.00	80.00	50.00	95.00	82.00	51.61
20	0.4	0.65	0.80	80.00	22.00	86.00	82.00	23.21
50	0.2	0.4	0.45	80.00	1.50	55.00	82.00	2.04

Note: $P_{VR,E}$ is the exceedance probability in 100 years for earthquake hazard.

684

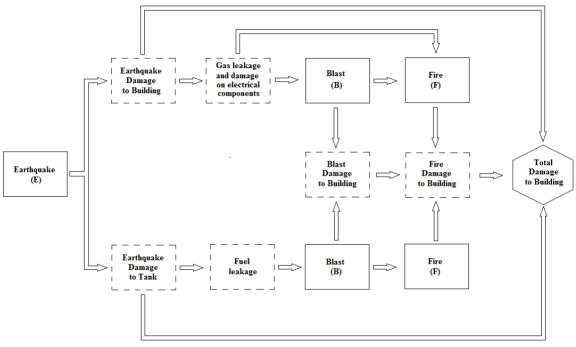| HAZARD	PROBABILITY OF EXCEEDING A GIVEN INTENSITY MEASURE
Hazard 1	$P(IM_1 \geq im_1)$
Hazard 2	$P(IM_2 \geq im_2) = P(IM_2 \geq im_2 \mid IM_1 \geq im_1) \cdot P(IM_1 \geq im_1)$
Hazard 3	$P(IM_3 \geq im_3) = P(IM_3 \geq im_3 \mid IM_2 \geq im_2) \cdot P(IM_2 \geq im_2 \mid IM_1 \geq im_1) \cdot P(IM_1 \geq im_1)$

Hazard analysis

$p(IM)$

hazards interaction

$p(IM_i \mid IM_{i-1})$

Structural analysis

$p(EDP \mid IM, SP)$

$p(EDP)$

Damage analysis

$p(DM \mid EDP)$

$p(DM)$

Loss analysis

$p(DV \mid DM)$

$p(DV)$

$p(SP)$

Structural characterization

Chain effects

Figure axes: Force (vertical axis, ranging from -1.2 to 1.2) versus Story Drift Ratio (horizontal axis, ranging from -0.08 to 0.08). Labeled points and slopes: E_i, E_f, $F_{R,i}$, $F_{R,f}$.

Section A-A

20 mm

2500 mm

2500 mm

1400 mm

500 mm

6 mm

50 mm

(a)   **(b)**   **(c)**

Axis labels:
- Vertical axis: $P(IM_B \geq im_B \mid IM_E \geq im_E)$ with values 0,00, 0,02, 0,04, 0,06, 0,08
- Left horizontal axis: **IM1:Sa(Ttank) [g]** with values 2,5, 2,0, 1,5, 1,0, 0,5, 0,0
- Right horizontal axis: **IM2:Fuel quantity [%]** with values 0, 20, 40, 60, 80, 100

CENTER LINE

H5

H4

H3

H2

H1

1.50

100%
92%
86%
80%

55%
62%
67%
70%
77%

2.00 m

(a)   **(b)**

(a)   **(b)**

(a)

(b)

(c)

(d)

Figure 9

(a)   **(b)**

Figure 18

(a)   **(b)**